ACS EARTH AND SPACE CHEMISTRY

Article

Cite This: ACS Earth Space Chem. XXXX, XXX, XXX−XXX

http://pubs.acs.org/journal/aesccq

Secondary Organic Aerosol Formation from Reaction of 3-Methylfuran with Nitrate Radicals

Taekyu Joo,[†] Jean C. Rivera-Rios,[‡] Masayuki Takeuchi,[§] Matthew J. Alvarado,[∥] and Nga Lee Ng*[,†,‡]

[†]School of Earth and Atmospheric Sciences, Georgia Institute of Technology, Atlanta, Georgia 30332, United States
[‡]School of Chemical and Biomolecular Engineering, Georgia Institute of Technology, Atlanta, Georgia 30332, United States
[§]School of Civil and Environmental Engineering, Georgia Institute of Technology, Atlanta, Georgia 30332, United States
[∥]Atmospheric and Environmental Research, Lexington, Massachusetts 02421, United States

Supporting Information

ABSTRACT: A significant amount of furan species is emitted from biomass burning. They are highly reactive to hydroxyl (OH) and nitrate radicals (NO_3), which can lead to the formation of secondary organic aerosol (SOA). Here, we investigate gas-phase oxidation and SOA formation from 3-methylfuran (C_5H_6O) via NO_3 reaction. Experiments are performed under dry conditions (RH < 5%) and with different initial concentrations of 3-methylfuran (from 95.9 to 562.8 ppb). We demonstrate that this reaction leads to SOA formation, with SOA yield ranging from 1.6 to 2.4% for organic mass loading ranging from 5.1 to 45 $\mu g/m^3$. More than half of the SOA mass is generated after complete depletion of 3-methylfuran, highlighting the importance of higher-generation or multiphase reactions to aerosol formation. Particle-phase organic nitrates contribute 39.4% of organics and their average volatility (average $C^* = 10^{-2.9}$ $\mu g/m^3$) is higher than that of non-nitrate organic compounds (average $C^* = 10^{-3.3}$ $\mu g/m^3$). A reaction mechanism is proposed based on the identified products, and $C_5H_5NO_5$ and $C_5H_6O_3$ are determined to be the major species in the gas and particle phases, respectively. Oligomer formation appears to determine the SOA composition and formation rate, and both gas-phase ROOR′ formation via $RO_2 + RO_2$ (acylperoxy radical) reactions and particle-phase accretion reactions can lead to the formation of the dimeric (C_{10}) compounds observed. Results from this study provide detailed chemistry of 3-methylfuran oxidation that can improve our understanding of its impact on SOA and ozone formation in nighttime biomass burning plumes.

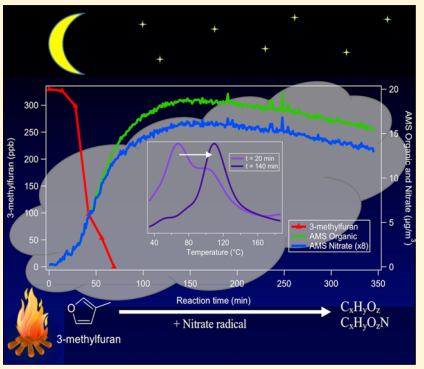

KEYWORDS: *Furan, methylfuran, biomass burning, secondary organic aerosol, SOA, oligomers, organic nitrate, nighttime oxidation*

INTRODUCTION

Biomass burning is a significant source of both gas- and particle-phase carbon in the atmosphere.[1−3] It impacts air quality and climate and is expected to increase due to climate change.[4] Biomass burning plumes contain thousands of nonmethane organic compounds (NMOCs) that can contribute to the formation of pollutants including ozone and secondary organic aerosol (SOA).[5,6] There has been substantial effort to identify these species and understand their behavior as the plumes age.[7−12] Recent studies have shown that furan compounds are an important class of NMOCs in biomass burning plumes, their contribution being higher in smoldering-type combustion than in flaming-type combustion.[9,13−15] Given their large emission rates and rapid reaction rates with hydroxyl (OH) and nitrate radicals (NO_3),[11,12,14,16] it is important to understand the atmospheric chemistry of furan derivatives. A few previous studies have shown the ability of these compounds to generate SOA.[17,18] However, their gas-phase oxidation products and mechanisms have not been identified and their SOA formation potential remains poorly constrained.

Furans are formed from cellulose pyrolysis,[19] and methylfurans are a major subset of furans, accounting for 20−25% of furan emissions.[13,14] Nighttime biomass combustion has been associated with variations in organic aerosol composition in multiple field campaigns, and in particular with the formation of organic nitrates.[20−23] Decker et al.[12] reported that furans can be responsible for 19−60% of initial NO_3 reactivity during nighttime biomass burning and around 60% of methylfurans are oxidized by NO_3 instead of OH or ozone. Tapia et al.[24] reported the rate coefficient and gas-phase products of 3-methylfuran oxidation by NO_3 radicals and proposed the gas-phase formation mechanism of first-generation organic nitrate products. However, the products were proposed based on the measurements of functional groups (rather than measurements of individual species) and SOA formation was not studied. For

Special Issue: New Advances in Organic Aerosol Chemistry

Received: March 20, 2019
Revised: April 21, 2019
Accepted: April 23, 2019
Published: April 23, 2019

DOI: 10.1021/acsearthspacechem.9b00068
ACS Earth Space Chem. XXXX, XXX, XXX−XXX

these reasons, there is a need to characterize the SOA formation potential and gas-phase chemistry of the 3-methylfuran + NO_3 reaction as it relates to nighttime aging in a biomass burning plume.

In this work, we investigate SOA formation from 3-methylfuran oxidation by NO_3 radicals in laboratory chamber experiments. SOA yields are determined from a series of experiments with different initial 3-methylfuran concentrations. Speciated gas-phase products and aerosol composition are monitored using online measurements in order to propose a mechanism for multigenerational oxidation and SOA formation. These results can be used to estimate SOA formation from biomass burning emissions and improve our understanding of oxidation in biomass burning plumes.

EXPERIMENTAL SECTION

Environmental Chamber Experiments. Experiments are performed in the Georgia Tech Environmental Chamber (GTEC) facility[25] at room temperature (~25 °C) and under dry conditions (<5% RH) (Table 1). Ammonium sulfate seed aerosol is introduced into the chamber by atomizing a 0.015 M solution. The initial particle number and volume concentrations are ~16 000 particles cm^{-3} and ~21 μm^3 cm^{-3}, respectively. In each experiment, 3-methylfuran (ACROS, Geel, Belgium) is injected into a glass bulb, and the compound is introduced into the chamber by passing pure air through the glass bulb.

Table 1. Experimental Condition and Aerosol Yield for All Experiments

Experiment	Condition	ΔHC (ppb)	ΔM_o ($\mu g/m^3$)	Yield (%)
1	3-methylfuran + NO_3	562.8 ± 2.2	45.0 ± 0.6	2.4 ± 0.03
2	3-methylfuran + NO_3	328.5 ± 1.2	24.0 ± 0.6	2.2 ± 0.06
3	3-methylfuran + NO_3	171.3 ± 0.3	10.6 ± 0.6	1.9 ± 0.1
4	3-methylfuran + NO_3	95.9 ± 0.2	5.1 ± 0.6	1.6 ± 0.2

After the seed particle and 3-methylfuran injection, NO_2 (Matheson, 500 ppm) and O_3 (generated by passing purified air through a UV radiation cell, Jelight 610, ~250 ppm) are injected into the chamber through a flow tube (0.9 L min^{-1} flow rate, 102 s residence time) in order to generate NO_3 radicals and N_2O_5.[25,26] NO_2 and O_3 react to form NO_3, which is followed by the reaction of NO_2 and NO_3 to form N_2O_5. N_2O_5 thermally decomposes back to NO_2 and NO_3 radicals establishing an equilibrium. To ensure >99% of 3-methylfuran reacts with NO_3 radicals instead of O_3 and to enhance the RO_2 + NO_3 channel, the concentration ratio of NO_2/O_3 is kept at ~5:3 and the 3-methylfuran/N_2O_5 ratio is targeted to be 1:4.

Gas-phase Measurements. The 3-methylfuran concentration is monitored using a gas chromatograph-flame ionization detector (GC-FID, Agilent 7890A) with a PLOT-Q column (Agilent). Oxidized reaction products are measured and reported as counts per second using a high-resolution time-of-flight chemical ionization mass spectrometer (HR-ToF-CIMS, Aerodyne Research Inc.) with iodide (I^-) as a reagent ion, which selectively measures polar or acidic compounds.[27−30] O_3 and NO_x are monitored using an O_3 Analyzer (Teledyne T400) and an ultrasensitive chemiluminescence NO_x monitor (Teledyne 200 EU), respectively.

Particle-phase Measurements. Size-dependent particle number and volume concentrations are monitored using a scanning mobility particle sizer (SMPS). The SMPS consists of a differential mobility analyzer (DMA) (TSI 3040) and a Condensation Particle Counter (CPC) (TSI 3775). A high-resolution time-of-flight aerosol mass spectrometer (HR-ToF-AMS, Aerodyne Research Inc.) measures bulk elemental composition of the particles (e.g., O/C and H/C ratios) and quantifies organics, nitrate, sulfate, ammonium, and chloride mass concentrations.[31,32] A Filter Inlet for Gases and AEROsol (FIGAERO, Aerodyne Research Inc.) inlet system is coupled with the HR-ToF-CIMS to detect particle-phase molecular composition.[26,33] FIGAERO allows particles to be collected onto a PTFE filter (Pall Corp, Zefluor 25 mm, 2 μm pore-size) for 20 min while measuring gas-phase species with the HR-ToF-CIMS. The particle-phase composition is analyzed through thermal desorption of the collected material (40 min total, including temperature ramping, soaking, and cooling cycle). FIGAERO-HR-ToF-CIMS provides insights into particle composition at the molecular level and aerosol volatility.[33,34] The volatility distribution of bulk organic aerosol, as saturation mass concentration (C^*, $\mu g\ m^{-3}$), is estimated based on the method used by Stark et al.[34] Briefly, a desorption temperature corresponding to the signal peak (T_{max}) is calibrated using compounds with known vapor pressures. The FIGAERO peak shape of the calibrated compounds is used to deconvolute the FIGAERO signal of the bulk aerosol using nonlinear multipeak fitting and to obtain the volatility distribution of the collected aerosol (Figure S-1).

RESULTS

SOA Formation from NO_3 Radical Oxidation of 3-Methylfuran. A series of experiments with different initial 3-methylfuran concentrations is performed to investigate the SOA formation potential of this system (Table 1). The initial 3-methylfuran concentrations ranges from 95.9 to 562.8 ppb. SOA formation is observed in all experiments and the particle wall loss-corrected[35] SOA mass yield (Y) ranges from 1.62% to 2.4% for an organic aerosol mass concentration (ΔM_o) of 5.1 to 45 $\mu g/m^3$ (Figure 1). A nucleation experiment is also conducted to determine SOA density. By comparing SMPS volume distribution and AMS mass distribution,[36] the SOA density is determined to be 1.24 g cm^{-3}. Although particle wall loss is corrected, the SOA yield reported here could represent the lower limit owing to vapor wall loss, where low volatility organic vapors could have partitioned to the chamber wall rather than to the aerosol.[37−41]

There was no prior study on SOA formation from 3-methylfuran + NO_3 but two previous studies reported SOA formation from 3-methylfuran + OH reaction. Alvarez et al.[17] reported a SOA yield of 8.5 ± 2.5% in the presence of 48 $\mu g/m^3$ of ΔM_o. Strollo and Ziemann[18] reported a similar average yield of 10%, but that corresponded to 2000−5000 $\mu g/m^3$ of ΔM_o implying a much lower SOA yield than that reported by Alvarez et al.[17] at 48 $\mu g/m^3$ of ΔM_o. In the context of these previous studies, we find that the SOA yield from NO_3 radicals oxidation is about a factor of 4 lower than the SOA yield from photooxidation reported by Alvarez et al. at similar ΔM_o values. In Figure 1a, SOA yield is parametrized as a function of organic mass produced using two types of fit: (1) a semiempirical model based on gas-to-particle partitioning of

DOI: 10.1021/acsearthspacechem.9b00068
ACS Earth Space Chem. XXXX, XXX, XXX−XXX

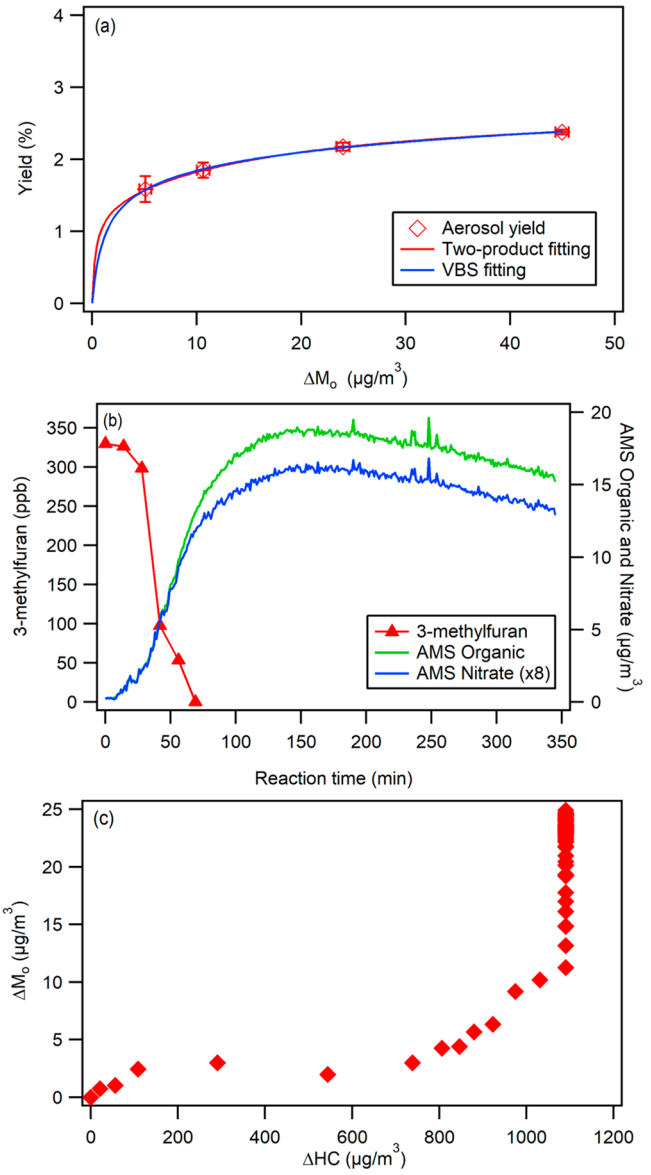

Figure 1. SOA yield and time profiles of 3-methylfuran oxidation and aerosol formation. (a) SOA yield and yield curve fitting using two-product model and VBS. (b) Reaction profile of an initial 3-methylfuran concentration of 328.5 ppb (Experiment #2 in Table 1). (c) Time-dependent growth curve. ΔM_o is calculated by the volume concentration measured with SMPS and SOA density, and ΔHC is obtained by interpolating GC-FID measurement to fit the time resolution between two measurements.

two semivolatile products[42,43] and (2) the volatility basis set (VBS) (eqs 1 and 2, respectively).[44] The fitting coefficients for both approaches are shown in Table 2.

$$Y = \Delta M_o \left[\frac{\alpha_1 K_1}{1 + K_1 M_o} + \frac{\alpha_2 K_2}{1 + K_2 M_o} \right] \quad (1)$$

$$Y = \Delta M_o \sum_i \frac{\alpha_i}{C_i^* + M_o} \quad (2)$$

Typical temporal profiles of the oxidation of 3-methylfuran are shown in Figure 1b,c. In addition to organics measured by the HR-ToF-AMS, the concentration of nitrate also increases steadily over the course of the experiment (Figure 1b). Since

Table 2. Fit Parameters of Two-Product Model and Volatility Basis Set[a]

(1) Two-product fitting				(2) VBS fitting		
α_1	K_1	α_2	K_2	α at C^* = 1	α at C^* = 10	α at C^* = 100
0.015	0.064	0.013	3.15	0.016	0.0067	0.01

[a] α = gas-phase mass fraction, unitless. K = partitioning coefficient, m^3 μg^{-1}. C^* = saturation vapor pressure, μg m^{-3}

inorganic nitrate formation via hydrolysis of N_2O_5 is not expected owing to the low RH during the course of the experiment, the observed increase can be attributed to the formation of organic nitrates. Figure 1c shows the time-dependent "growth curve" (ΔM_o as a function of hydrocarbon consumed, ΔHC).[45,46] The vertical section indicates that more than half of the SOA is formed after all the 3-methylfuran is consumed. These results demonstrate that there is a substantial contribution from multigenerational oxidation and/or heterogeneous/multiphase reactions to SOA formation.

Bulk Composition of SOA. A typical HR-ToF-AMS aerosol mass spectrum is shown in Figure S-2. The signals at m/z 39 ($C_3H_3^+$), m/z 68 ($C_4H_4O^+$), m/z 69 ($C_4H_5O^+$), m/z 82 ($C_5H_6O^+$), m/z 97 ($C_5H_5O_2^+$), and m/z 44 (CO_2^+) are particularly high. The signal at m/z 82 is a well-known isoprene SOA signature as determined by positive matrix factorization (PMF) analysis of AMS data.[47−53] Here, m/z 82 constitutes 1% of total organics (Figure S-2). Structural similarities between 3-methylfuran + NO_3 products and isoprene SOA could be the reason for the observed enhancement in m/z 82. Specifically, Lin et al.[49] proposed that 3-methyltetrahydrofuran-3,4-diols associated with IEPOX-SOA can form methylfuran-like structures when decomposed in the AMS. The enhancement of m/z 44 (CO_2^+) can be an indicator of the presence of organic acids in the SOA.[54−57] HR-ToF-AMS nitrate-to-organics ratio is 0.11, where nitrate mainly comes from NO^+ and NO_2^+ fragments. The NO^+/NO_2^+ (NO_x^+) ratio ranges from 5.1 to 5.4 throughout all the experiments in this study, which is within the range that indicates the presence of organic nitrates as reported in previous studies.[25,51,58−62]

Speciated Gas- and Particle-phase Chemical Composition. The mass spectrum of gas- and particle-phase compounds obtained from the HR-ToF-CIMS at the peak aerosol growth is shown in Figure 2, where both organic nitrates and non-nitrate organic species are detected. $C_5H_5NO_5I^-$ (m/z 286) is the strongest signal among the 18 major gas species, around 20 times higher than the other compounds (Figure 2a). $C_5H_6O_3I^-$ (m/z 241) is the next most abundant gas species, which is 5% of the $C_5H_5NO_5I^-$ signal, and the others are ≤2% of the $C_5H_5NO_5I^-$ signal. In the particle phase, however, $C_5H_5NO_5I^-$ is a minor compound while $C_5H_6O_3I^-$ is the highest among the 224 organic ions detected. Compounds with five or fewer number of carbons are mostly distributed below 330 m/z (green region in Figure 2b), and compounds with six or higher number of carbons are mostly distributed over 330 m/z (blue region in Figure 2b), which are classified as the oligomer region. The six major species in each region (Figure 2b-i,b-ii) account for 68% of the total signal of FIGAERO-identified species in the particle phase. The particle-phase ions detected by the FIGAERO-HR-ToF-CIMS could potentially include the fragments resulting from thermal decomposition of particles.[63,64] Therefore, the

DOI: 10.1021/acsearthspacechem.9b00068
ACS Earth Space Chem. XXXX, XXX, XXX−XXX

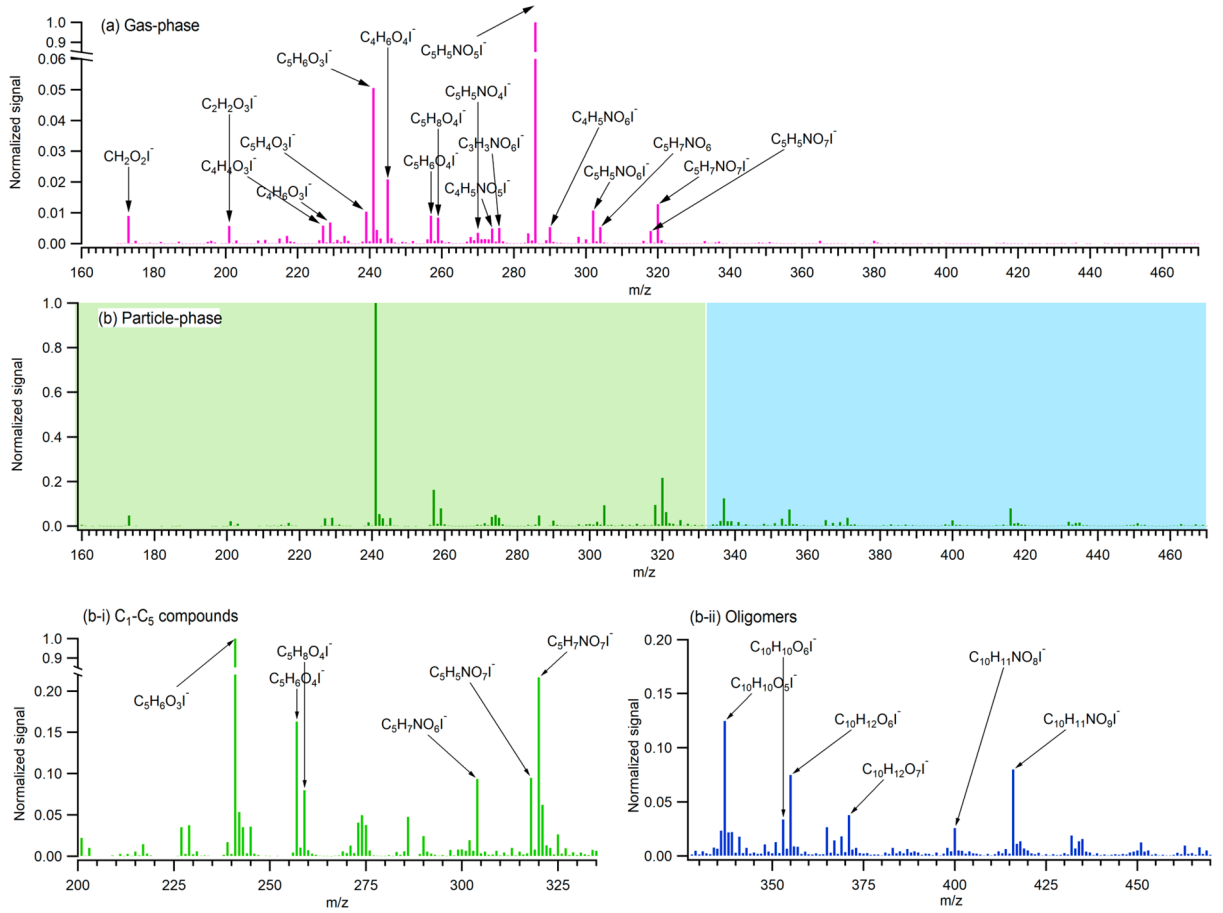

Figure 2. HR-ToF-CIMS mass spectra of (a) gas-phase and (b) particle-phase for a typical experiment (Experiment #2 in Table 1). The *m*/*z* include the mass of the I^- ion (i.e., *m*/*z* = 126.905). (b-i) Mass spectrum of C_1-C_5 compounds (green box region in (b)), and (b-ii) mass spectrum of oligomers in the particle phase (blue box region in (b)).

specific types of C_5 compounds detected can correspond to parent molecules and/or thermal decomposition of higher molecular weight oligomers.

Figure 3 shows the time evolution of selected gas- and particle-phase species measured by the FIGAERO-HR-ToF-CIMS. Gas-phase compounds detected by the HR-ToF-CIMS showed two different patterns in the time traces. $C_5H_5NO_5I^-$ and $C_5H_7NO_6I^-$ in Figure 3a increase rapidly once N_2O_5 is injected and stay constant after all the 3-methylfuran is consumed, which is characteristic of first-generation gas-phase oxidation products. The signal for other species increases slowly and steadily until the end of the experiment (Figure 3b), which is characteristic of later-generation products. $C_5H_6O_3I^-$ is an exception as seen in Figure 3b, where the signal is stabilized after all the 3-metylfuran is consumed. The time series data suggest that this compound is a multigenerational product: (1) Unlike $C_5H_5NO_5I^-$ and $C_5H_7NO_6I^-$ (first-generation products), $C_5H_6O_3I^-$ does not show an immediate increase upon onset of oxidation and (2) it continues to increase after N_2O_5 injection is stopped. These two observations are consistent with the proposed mechanism that $C_5H_6O_3$ is a second-generation product (see discussion in later sections). The six major C_5 and C_{10} particle-phase compounds show similar time evolutions as the bulk aerosol mass concentration (Figure 3c,d). In general, C_{10} compounds reach the maximum with a faster rate than the most of the C_5 compounds. For both C_5 and C_{10} compounds, the non-nitrate organics increase at a faster rate than the nitrate compounds. Since low-volatility species will readily partition into the particle phase,[43,44,65] this observation suggests that non-nitrate organic compounds could be less volatile than nitrate compounds.

Saturation Vapor Pressure Evolution and SOA Contribution by Carbon Number. The time evolution of FIGAERO thermograms for SOA products with different carbon number is shown in Figure 4. The thermograms of C_1-C_5, C_6-C_{10}, and $C_{11}-C_{18}$ compounds show a similar pattern throughout the experiment. C_1-C_5 compounds contribute most of the total particle-phase signal in Figure 4, and $C_5H_6O_3$ (green triangles) alone contributes ~40% of the C_1-C_5 signal throughout the experiment. All thermograms in Figure 4 show a multiple-peak pattern, indicating the presence of both monomers and oligomers in SOA.[33,64,66] The multiple-peak pattern is more obvious at t = 20 min. The T_{max} of the largest peak appears at ~70 °C during the first FIGAERO cycle (t = 20 min), shifts to ~110 °C at the maximum aerosol mass (t = 140 min), and remains the same until the end of the experiment (t = 320 min). The evolution of the SOA volatility distribution is also shown in Figure 4. At t = 20 min, the SOA includes both semivolatile and low-volatility species. The volatility distribution of SOA shows a peak at C^* = 10^{-1} μg m^{-3} and is fairly evenly spread out across other bins. The peak shifts to C^* = 10^{-4} μg m^{-3} at t = 140 min (maximum aerosol mass) and stays the same afterward.

DOI: 10.1021/acsearthspacechem.9b00068
ACS Earth Space Chem. XXXX, XXX, XXX−XXX

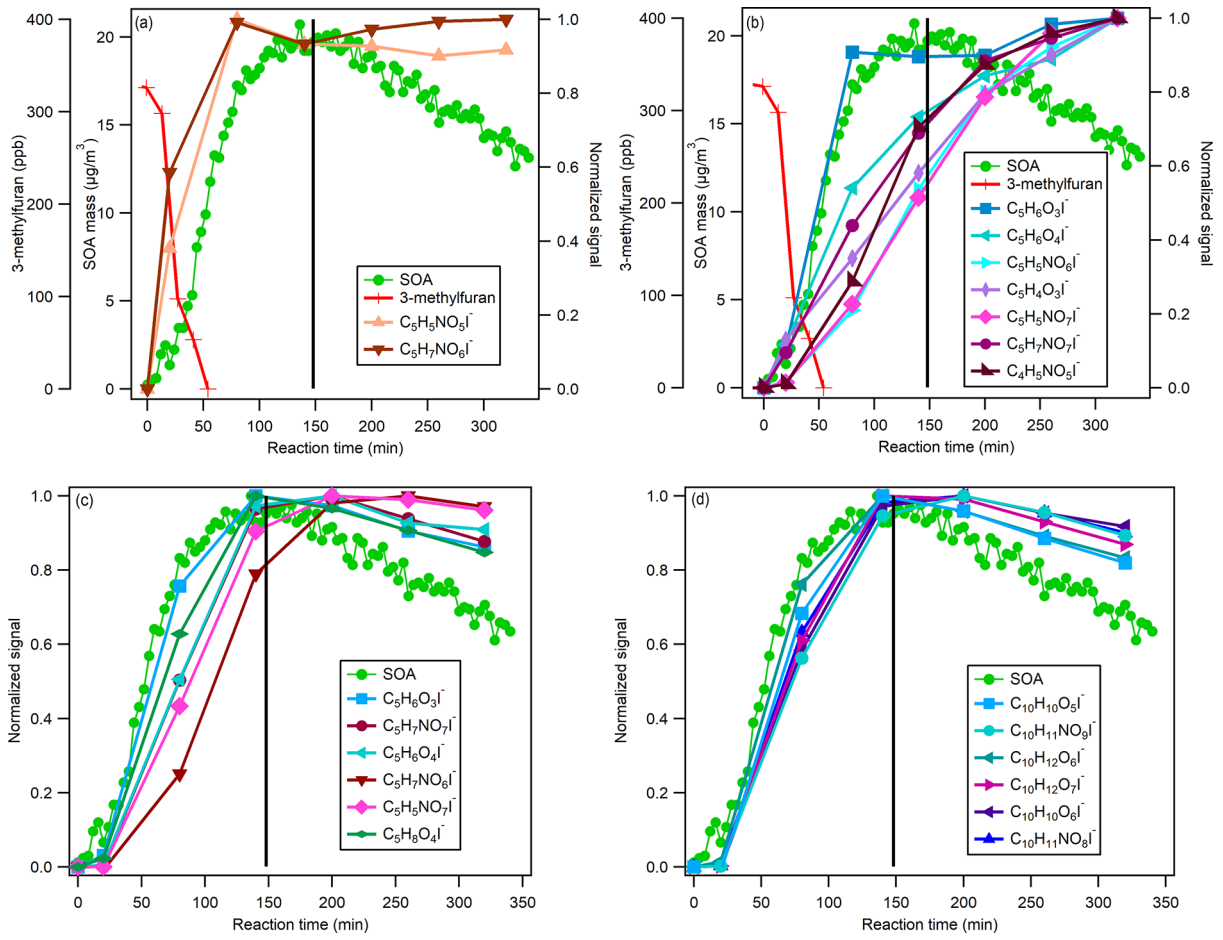

Figure 3. Time series of gas- and particle-phase species from HR-ToF-CIMS (Experiment #2 in Table 1). The top two panels are gas-phase time series and the bottom two panels are particle-phase time series. (a) Time series of first-generation products and (b) Time series of later generation products. (c) Time series of major C_5 compounds and (d) Time series of major C_{10} compounds. The time series of 3-methylfuran and SOA formation (calculated from SMPS volume concentration and SOA density) are also shown for reference. The black line represents the time when N_2O_5 injection is terminated. The signals are normalized by the maximum signal of each species throughout the experiment.

DISCUSSION

Mechanism of 3-Methylfuran Oxidation by NO_3 Radical. Figure 5 shows a proposed mechanism for the reaction of 3-methylfuran with NO_3 radicals based on the observed oxidation products. The formation of first- and higher-generation products in the proposed mechanism are consistent with the time evolutions of the species shown in Figure 3. The reaction starts with the addition of $-ONO_2$ to the 2 or 5 position, which are favored due to the stability of the resulting radical.[18,24,67] The cyclic nitrooxyalkyl radical can either react with O_2 to form a cyclic nitrooxyperoxy radical (RO_2,PR1) or lose NO_2 and become 2-methylbutenedial (**1**), a first-generation product that has been shown to form in high yield (38−83%) from both OH radical and NO_3 radical oxidations.[17,24,68,69] The other first-generation products 2, 3, and 4 proposed in Figure 5 are formed via reaction of PR1. PR1 reacts with HO_2 to form nitrooxy hydroperoxide ($R(ONO_2)OOH$, $C_5H_7NO_6$) (**4**) or reacts with $NO_3/HO_2/RO_2$ to form nitrooxyalkoxy radical ($R(ONO_2)O$, AR1). Tapia et al.[24] proposed the formation of peroxydinitrate ($R(ONO_2)(OONO_2)$), nitrooxy carbonyl ($R(ONO_2)(O)$), and nitrooxy alcohol ($R(ONO_2)(OH)$) from AR1, but these reaction pathways are not included owing to their low signals in the HR-ToF-CIMS (Figure 2a) or their slow formation rates relative to other pathways as shown in Figure S-4. AR1 can undergo further reaction to form $C_5H_5NO_5$, which is the major gas-phase product detected by the HR-ToF-CIMS (Figure 2a). There are two possible isomers of $C_5H_5NO_5$ from AR1: ring-opened nitrooxy dicarbonyl ($R(ONO_2)(O)(O)$) (**2**) and cyclic nitrooxy carbonyl ($R(ONO_2)(O)$) (**3**) via decomposition and reaction of AR1 with O_2, respectively. The formation of isomer **2** is expected to be favored because the decomposition pathway is estimated to be eight orders of magnitude faster than the reaction with O_2 (Figure S-4).

A suite of second-generation products is formed from reactions of compounds **1** and **2**. Compound **1** reacts with NO_3 and forms acylperoxy radical ($R(O)O_2$, PR2) or tertiary nitrooxyperoxy radical (PR3) via H-abstraction from aldehyde or addition to the C=C double bond, respectively. Among these two pathways, the formation of PR2 will be favored because the aldehyde groups reduce the reactivity of the double bond and Rayez et al.[70] reported that the H-abstraction from an aldehyde is always dominant relative to the addition to the double bond in an alkenal. Further oxidation of compound **2** results in the formation of nitrooxy carbonyl acylperoxy radical (PR4). In general, the fates of the PR1−4 depend on their reaction partners: $RO_2 + NO_3$, $RO_2 + RO_2$, $RO_2 + HO_2$, $RO_2 + NO_2$, $RO_2 + NO$, and RO_2 isomerization. Under the reaction conditions in this study, the $RO_2 + NO_3$ channel is

DOI: 10.1021/acsearthspacechem.9b00068
ACS Earth Space Chem. XXXX, XXX, XXX−XXX

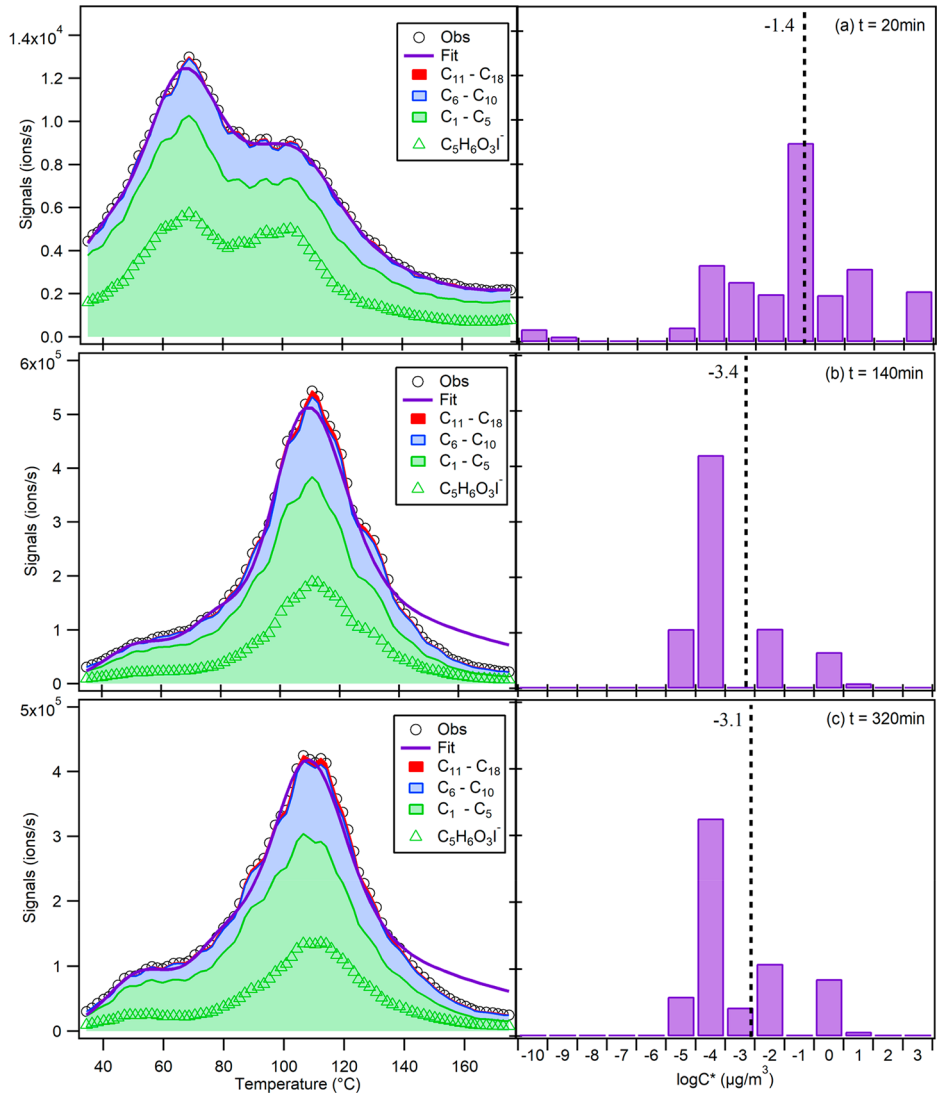

Figure 4. Time evolution of thermogram for total SOA, C_1-C_5 compounds, C_6-C_{10} compounds, and $C_{11}-C_{18}$ compounds over the course of a typical experiment (Experiment #2 in Table 1). The dotted line represents the log-weighted averaged C*. (a) Beginning of the oxidation. (b) Peak aerosol growth. (c) End of the experiment. Saturation vapor pressure is calculated from the FIGAERO calibration. The difference between observation and fitting (tail) in the middle and bottom panels is due to the shape of thermogram obtained during FIGAERO calibration (Figure S-1). Signals at log C* of −10 and −9 $\mu g/m^3$ at t = 20 min are due to the interference from the background.

expected to dominate, though RO_2 + RO_2 and RO_2 + HO_2 reactions and the corresponding products are also detected by the HR-ToF-CIMS.

In Figure 5, compounds **5**−**12** are formed via further reactions of PR2 or PR3, and compounds **13** and **14** are formed via further reactions of PR4. PR2 can react with NO_2 to form organic acyl peroxynitrate ($R(O)OONO_2$, $C_5H_5NO_6$) (**5**) and with HO_2 to form peroxy acid ($R(O)OOH$, $C_5H_6O_4$) (**6**) or organic acid ($RCOOH$, $C_5H_6O_3$) (**7**). Compound **7** can also be produced through RO_2 + RO_2 reactions.[71,72] PR2 can also react with NO_3, HO_2, or RO_2 to form acylalkoxy radical ($R(O)O$, AR2). AR2 can then decompose to form cyclic dicarbonyl ($R(O)(O)$, $C_5H_4O_3$) (**8**) or isomerize to form carboxylic acyl peroxy radical (PR5) that reacts further to form dicarboxylic acid ($R(COOH)COOH$, $C_5H_6O_4$) (**9**) and carboxylicperoxyacylnitrate ($R(COOH)(O)OONO_2$, $C_5H_5NO_7$) (**10**). Among these two reaction branches, it is expected that the isomerization pathway would be favored because the H-abstraction rate from the aldehyde is two orders of magnitude faster than the decomposition rate (Figure S-4). As for PR3, it can react with HO_2 to form nitrooxy hydroperoxide (**11**) or with $RO_2/NO_3/HO_2$ to form nitrooxy alkoxy radical (AR3) and subsequently decompose to C_4 nitrooxy dicarbonyl ($R(ONO_2)(O)(O)$, $C_4H_5NO_5$) (**12**). Lastly, further reactions of PR4 lead to the formation of nitrooxy peracetic acid ($R(ONO_2)(O)OOH$, $C_5H_5NO_7$) (**13**) and nitrooxy carboxylic acid ($R(ONO_2)COOH$, $C_5H_5NO_6$) (**14**).

Multigenerational Chemistry in SOA Formation. As seen in Figure 1b,c, there is continuous SOA formation after the complete depletion of 3-methylfuran. The particle mass spectrum measured by FIGAERO-HR-ToF-CIMS indicates the presence of dimers (Figure 2) and various gas- and particle-phase species continue to increase over the course of the experiment (Figure 3). The continued SOA formation can be due to gas-particle partitioning of higher-generation gas-phase products and/or further particle-phase reactions. We highlight the species $C_5H_6O_3$ here as it is the most abundant

DOI: 10.1021/acsearthspacechem.9b00068
ACS Earth Space Chem. XXXX, XXX, XXX−XXX

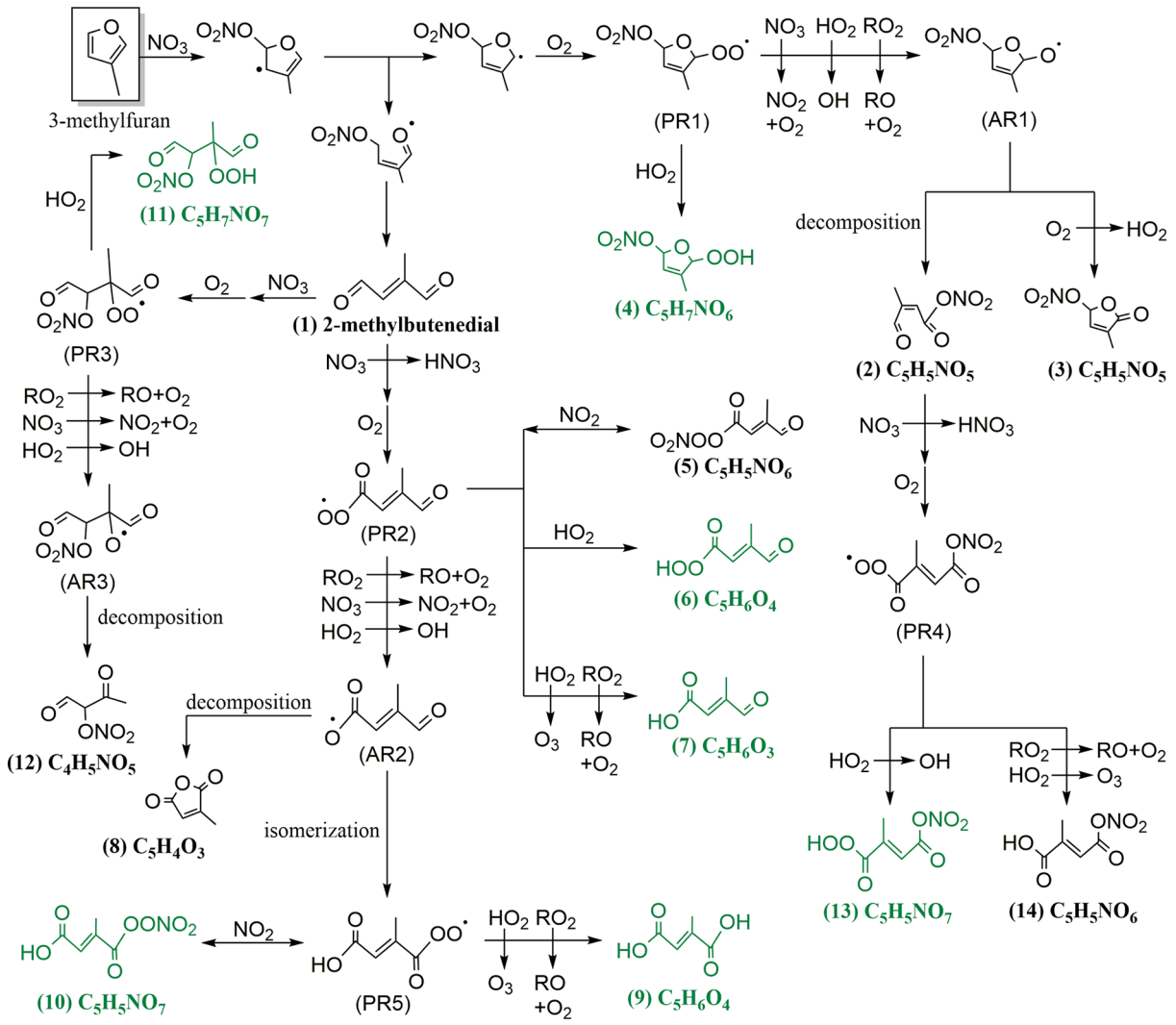

Figure 5. Proposed mechanism for 3-methylfuran oxidation by NO_3 radicals. Selected particle species in Figure 2 is colored in green. NO_3 can be added to 2 or 5 position, but addition to 5 position is shown here as the representative case.

species detected in the particle phase. There are multiple pathways that could lead to the formation of $C_5H_6O_3$, which include multigenerational oxidation and particle-phase reaction: (1) further gas-phase oxidation of the first-generation product 2-methylbuteneidal, (2) decomposition from oligomers, and (3) functional group conversion through particle-phase reactions. The 2-D thermogram[73] in Figure S-3 shows similar T_{max} for species with a wide range of molecular weights, which could indicate that lower molecular weight compounds are thermal decomposition products of high molecular weight compounds. For instance, $C_5H_6O_3$, which is detected as the major compound in the particle phase, is estimated to have $C^* = 10^{4.4}$ $\mu g\ m^{-3}$ by simple group contribution method (SIMPOL),[74] which is much more volatile than the C* value estimated from the thermogram in Figure 4 ($C^* = 10^{-4}$ $\mu g\ m^{-3}$). It is likely that the C* estimated by the group contribution method is biased high and that $C_5H_6O_3$ arises from thermal decomposition of lower volatility oligomers during the FIGAERO cycle.[34]

We propose a set of particle-phase accretion reactions from the six C_5 compounds with the highest signal intensities that can lead to the formation of C_{10} dimers (Figure S-5). The particle-phase accretion reactions require functionalized compounds, which are either 2-methylbutenedial or its reaction products as shown in Figure 5.[75,76] The C_{10} compounds can also be generated via gas-phase ROOR′ formation ($RO_2 + RO_2$) from acylperoxy radicals. Although it has been reported that ROOR′ formation is uncertain[77] and is a minor pathway,[78−80] the branching ratio of ROOR′ formation could be higher here because the larger RO_2 in this study would have more vibrational modes that can distribute collisional energy to prevent breakage of ROOR′.[81] All proposed dimers in Figure S-5 share similar backbone with $C_5H_6O_3$, which could lead to the enhancement in $C_5H_6O_3$ signal during the thermal desorption cycle of the FIGAERO as dimers break down to from $C_5H_6O_3$. The proposed dimers can also further react and undergo Baeyer−Villiger reactions that can lead to the formation of carboxylic acids,[82] which could contribute to $C_5H_6O_3$ signal.

The time evolution of the thermograms of particle-phase species (Figure 4) also indicate that multigenerational or multiphase reactions are contributing to SOA formation. As the variation in the shape of the thermogram is related to the evolution in the saturation vapor pressure of SOA, this indicates that volatile species ($C^* \approx 10^{-1}$ $\mu g\ m^{-3}$) are contributing to SOA formation at the beginning of the

DOI: 10.1021/acsearthspacechem.9b00068
ACS Earth Space Chem. XXXX, XXX, XXX−XXX

experiment, and further reactions continue to generate less-volatile species (C* ≈ 10^{-4} μg m^{-3}) over the course of the experiment. This is in agreement with the changes in O/C ratio measured by the HR-ToF-AMS in Figure S-6. It has been reported that O/C ratio and volatility of SOA are anticorrelated in general,[83−86] thus increasing O/C ratio over the course of the experiment is consistent with the presence of more low-volatility species in SOA over time. After peak aerosol growth, however, the thermogram shows relatively small changes (slight decrease of signal and peak broadening) until the end of the experiment (Figure 4c). The O/C ratio also shows relatively small changes compared to the variation before reaching the peak aerosol growth (Figure S-6). This may indicate that the aging processes over the course of the experiment do not alter bulk SOA characteristics and O/C to a large extent.

Organic Nitrates Formation. As mentioned in the previous section, the HR-ToF-AMS mass spectrum in Figure S-2 indicates the presence of nitrate species. Farmer et al.[59] suggested that NO_x^+ is higher for organic nitrates than inorganic nitrates. In all the furan experiments in this study, the NO_x^+ for organic nitrates (R_{ON}) ranges from 5.1 to 5.4, which is higher than the NO_x^+ that is measured by atomizing pure ammonium nitrate into the AMS (R_{AN} = 3.8) in our study. The R_{ON} observed in the furan experiments is comparable to the isoprene + NO_3 system (R_{ON} = 5) but smaller than the R_{ON} of monoterpene + NO_3 system (R_{ON} = 6.5−15).[25,26,58,60,62] However, the corresponding R_{ON}/R_{AN} ratio (∼1.4 in this study), which was proposed by Fry et al.[87] to constrain instrumental bias, is lower than both isoprene + NO_3 (R_{ON}/R_{AN} = 2.1) and monoterpene + NO_3 (R_{ON}/R_{AN} = 3.7−4.2) systems in previous studies.[25,60]

We estimate the fraction of particle-phase organic nitrates in organics to be 39.4% using the observed nitrate-to-organics mass ratio (0.11) measured by the HR-ToF-AMS. The molecular weight of particle-phase organic nitrates needs to be considered in order to estimate the fraction of organic nitrates in organic aerosol. Based on the speciated particulate organic nitrates measured by the FIGAERO-HR-ToF-CIMS, the signal-weighted average organic nitrate molecular weight is approximated to be 222 g mol^{-1}.

The fraction of organic aerosol composed of organic nitrates is generally lower than previously reported values from monoterpene + NO_3 (56−80%).[25,26,61,88] However, since furans are highly reactive toward NO_3 radicals,[11,12] this could indicate that furan + NO_3 reactions during biomass burning can be an important source of particulate organic nitrates, which is a NO_x reservoir in the atmosphere.[61]

Volatility of SOA. As shown in the FIGAERO thermogram in Figures 4 and S-7, about 55% of the SOA at t = 140 min and t = 320 min has a C* ≤ 10^{-4} μg m^{-3}. This observed volatility range corresponds to extremely low-volatility organic compounds (ELVOCs) or low-volatility organic compounds (LVOCs), which can readily partition into the aerosol.[89,90] The volatility of the total 3-methylfuran + NO_3 SOA is lower than that of the ambient biomass burning OA (BBOA), which is reported to mostly consist of semivolatile organic compounds (SVOCs) or LVOCs.[91−94] Ambient BBOA can consist of primary and/or secondary OA, which can have different volatilities. The lower volatility in this study is likely due to the higher contribution from secondary chemistry to OA concentration. We believe C_{15} or higher compounds contribute to SOA composition since the C* of selected C_5 and C_{10} compounds, estimated using SIMPOL,[74] ranges from 10^2 to 10^5 μg m^{-3} and 10^{-2} to 10^1 μg m^{-3}, respectively. This is much more volatile than the observed volatility distribution for C_5 compounds as shown.

The yield-based VBS fitting parametrizes mass fraction at C* = [1, 10, 100 μg m^{-3}] (Figure 1a and Table 2), which is different from the FIGAERO-based values in Figure S-7 and Table S-1 (C* from 10^{-5} to 10^1 μg m^{-3}). We note that the VBS-fitting corresponds to data from all experiments, which include compounds of differing volatility in experiments with lower and higher organic loadings, while the FIGAERO-based estimation uses data from one specific experiment (Experiment 2 in Table 1). Nevertheless, one can still obtain some insights from the difference in aerosol volatility derived using VBS-fitting vs FIGAERO. In general, the mass concentrations in the higher-volatility bins (10 and 100 μg m^{-3}) from the yield-based VBS fitting are higher than those from FIGAERO-based estimations. It is possible that this is a result of FIGAERO preferentially detecting compounds of relatively lower volatility with the use of I^- as reagent ion. We find that the mass concentration that corresponds to the least volatile bin C* = 1 μg m^{-3} (17.64 μg m^{-3}, Table 2) from VBS-fitting is not substantially different from the integrated mass from C* of 10^{-10} to 10^{-3} μg m^{-3} (16.97 μg m^{-3}, Figure S-7 and Table S-1) in FIGAERO data. Thus, it appears that ELVOC and LVOC masses measured by FIGAERO have been allocated into the C* = 1 μg m^{-3} bin in the yield-based VBS fitting. Our observations are consistent with Saha and Grieshop,[95] who reported that yield-based VBS fitting may overestimate the contribution from SVOCs compared to thermal desorption method and lead to underestimation of the SOA mass yield particularly at low organic mass loading.

The volatility distributions of particulate organic nitrates and non-nitrate organics are compared in Figure S-8. The C* of organic nitrates is more evenly distributed across all volatility bins, especially with more contribution from higher volatility bins compared to non-nitrate organics. About 55% and 66% of organic nitrates and non-nitrate organics have C* ≤ 10^{-4} μg m^{-3}, respectively. Overall, the average C* of organic nitrates and non-nitrate organics is $10^{-2.9}$ and $10^{-3.3}$ μg m^{-3}, respectively. Such volatility difference is consistent with the time evolutions in Figure 3c,d where nitrated compounds reach peak aerosol growth at a later time than non-nitrate organic compounds.

A few prior studies have reported on the volatility of organic nitrates. The volatility of bulk organic nitrates from 3-methylfuran + NO_3 is generally lower than organic nitrates from β-pinene + NO_3 oxidation (∼$10^{1.7}$ μg m^{-3}).[58] However, comparison of the volatility of particle-phase organic nitrates should be carefully considered since the volatility in Fry et al.[58] was estimated using a partitioning and group contribution method, which is different from this study. Field studies reported that polymerized organic nitrates could exist in the low-volatility region,[96] but further studies are required to understand the underlying chemistry leading to these species.

■ ATMOSPHERIC IMPLICATIONS

To our knowledge, this work is the first study to demonstrate SOA and particle organic nitrates formation from the 3-methylfuran + NO_3 reaction. There have been a few studies focusing on SOA formation from gas-phase oxidation of biomass burning emissions but studies that reported nighttime oxidation of biomass burning precursors are much more

DOI: 10.1021/acsearthspacechem.9b00068
ACS Earth Space Chem. XXXX, XXX, XXX−XXX

limited even though nighttime oxidation also has the potential to form SOA. Hartikainen et al.[11] observed an inverse correlation between furans and organic aerosol mass in the flame chamber experiments and proposed that furans can potentially be a major group of SOA precursors. Here, we report a series of chamber experiments with an initial 3-methylfuran concentration of 95.9 to 562.8 ppb under dry conditions at room temperature. SOA yield ranges from 1.6 to 2.4% for 5−45 $\mu g\ m^{-3}$ of organic aerosol mass. Previous studies reported that furans can account for 10−50% of the potential SOA formed during daytime oxidation of biomass burning plume when an assumed 10% SOA yield is applied for all furans.[18,97] Considering the relatively large emission rates of furans during biomass burning, a 2% SOA yield from this study suggests that furans can potentially be an important nighttime SOA precursor. If typical nighttime RH conditions are considered, which are higher than in this study, the SOA yield may increase owing to oligomerization or reactive uptake of water-soluble compounds.[48,75,98] Future studies are warranted to investigate SOA formation from furan oxidation under various reaction conditions.

Higher-generation oxidation products and possibly multiphase accretion reactions contribute significantly to SOA formation from the 3-methylfuran + NO_3 reaction. There are two lines of evidence to support this: (1) SOA continues to increase after 3-methylfuran is completely oxidized and (2) the volatility bin that contributes the most to the SOA is $C^* = 10^{-4}$ $\mu g\ m^{-3}$, which is much lower than the volatility expected from C_5 compounds. One of the main gas-phase products expected from the 3-methylfuran + NO_3 reaction is 2-methylbutenedial.[17,24,69] The results from the HR-ToF-CIMS indicate that further oxidation of 2-methylbutenedial can contribute to SOA significantly. This is likely due to the formation of acylperoxy radicals when 2-methylbutenedial reacts with NO_3. The slow N_2O_5 injection used in this study as well as the fact that these radicals have some of the fastest RO_2 + RO_2 reaction rates can lead to considerable dimer formation (ROOR′) and multifunctional species. The aldehyde groups can also participate in accretion reactions or be oxidized to carboxylic acids in the condensed phase. The molecular formulas of the observed products imply that the compounds in the particle phase are multifunctional and likely to engage in accretion reactions. If other VOCs in biomass burning plumes have similar products, it is expected that these compounds will form SOA efficiently through multigeneration and multiphase chemistry.

3-Methylfuran + NO_3 reaction can impact O_3 formation as well. In addition to ROOR′ formation, acylperoxy radicals can form acylperoxy nitrates via reaction with NO_2, which can act as NO_x reservoirs during biomass burning.[99] Another NO_x reservoir that is formed during the 3-methylfuran + NO_3 oxidation are particle-phase organic nitrates, which contribute 39.4% of the organics. Both acylperoxy nitrates and particle organic nitrates can participate in NO_x recycling via thermal dissociation and hydrolysis/photochemical loss, respectively.[25,26,61] Recent studies have shown that particulate organic nitrates are ubiquitous in the atmosphere.[61] Considering 3-methylfuran is highly reactive with NO_3 radicals, this work highlights the potential importance of organic nitrates sources outside of traditional VOCs.

Although it has been reported in some previous studies that net OA mass addition in biomass burning plumes can be small, the degree of oxidation of aerosol has been found to increase with photochemical evolution, indicating the strong influence and importance of secondary chemistry.[100−105] The results in this study provide detailed nighttime chemistry and SOA formation from 3-methylfuran oxidation and improve our understanding of the chemical evolution of biomass burning plumes.

■ ASSOCIATED CONTENT

Supporting Information

The Supporting Information is available free of charge on the ACS Publications website at DOI: 10.1021/acsearthspacechem.9b00068.

FIGAERO volatility calibration curve, AMS organic mass spectrum, 2-D thermogram from FIGAERO-HR-ToF-CIMS, description of the mechanism and reaction rate of radicals, possible dimer formation reactions, variation of O/C ratio, organic mass concentration for each volatility bin, and thermogram of nitrate and non-nitrate organic compounds and their saturation vapor pressure estimation (PDF)

■ AUTHOR INFORMATION

Corresponding Author

*E-mail: ng@chbe.gatech.edu.

ORCID

Taekyu Joo: 0000-0002-8252-4232

Nga Lee Ng: 0000-0001-8460-4765

Notes

The authors declare no competing financial interest.

■ ACKNOWLEDGMENTS

This research was funded by NSF AGS-1830727. The FIGAERO-HR-ToF-CIMS was purchased with NSF Major Research Instrumentation (MRI) grant 1428738. The authors would like to thank T. Berkemeier and F. Liu for helpful discussions.

■ REFERENCES

(1) Crutzen, P. J.; Andreae, M. O. Biomass burning in the tropics: Impact on atmospheric chemistry and biogeochemical cycles. *Science* **1990**, *250* (4988), 1669−1678.

(2) Akagi, S.; Yokelson, R. J.; Wiedinmyer, C.; Alvarado, M.; Reid, J.; Karl, T.; Crounse, J.; Wennberg, P. Emission factors for open and domestic biomass burning for use in atmospheric models. *Atmos. Chem. Phys.* **2011**, *11* (9), 4039−4072.

(3) Reddington, C. L.; Spracklen, D. V.; Artaxo, P.; Ridley, D. A.; Rizzo, L. V.; Arana, A. Analysis of particulate emissions from tropical biomass burning using a global aerosol model and long-term surface observations. *Atmos. Chem. Phys.* **2016**, *16* (17), 11083−11106.

(4) Abatzoglou, J. T.; Williams, A. P. Impact of anthropogenic climate change on wildfire across western US forests. *Proc. Natl. Acad. Sci. U. S. A.* **2016**, *113* (42), 11770−11775.

(5) Alvarado, M. J.; Prinn, R. G. Formation of ozone and growth of aerosols in young smoke plumes from biomass burning: 1. Lagrangian parcel studies. *J. Geophys. Res.* **2009**, *114*, D09306.

(6) Alvarado, M.; Lonsdale, C.; Yokelson, R.; Akagi, S. K.; Coe, H.; Craven, J.; Fischer, E.; McMeeking, G.; Seinfeld, J.; Soni, T. Investigating the links between ozone and organic aerosol chemistry in a biomass burning plume from a prescribed fire in California chaparral. *Atmos. Chem. Phys.* **2015**, *15* (12), 6667−6688.

(7) Grieshop, A.; Logue, J.; Donahue, N.; Robinson, A. Laboratory investigation of photochemical oxidation of organic aerosol from wood fires 1: measurement and simulation of organic aerosol evolution. *Atmos. Chem. Phys.* **2009**, *9* (4), 1263−1277.

DOI: 10.1021/acsearthspacechem.9b00068
ACS Earth Space Chem. XXXX, XXX, XXX−XXX

(8) Bruns, E. A.; El Haddad, I.; Slowik, J. G.; Kilic, D.; Klein, F.; Baltensperger, U.; Prévôt, A. S. H. Identification of significant precursor gases of secondary organic aerosols from residential wood combustion. *Sci. Rep.* **2016**, *6*, 27881.
(9) Hatch, L. E.; Yokelson, R. J.; Stockwell, C. E.; Veres, P. R.; Simpson, I. J.; Blake, D. R.; Orlando, J. J.; Barsanti, K. C. Multi-instrument comparison and compilation of non-methane organic gas emissions from biomass burning and implications for smoke-derived secondary organic aerosol precursors. *Atmos. Chem. Phys.* **2017**, *17* (2), 1471−1489.
(10) Fang, Z.; Deng, W.; Zhang, Y.; Ding, X.; Tang, M.; Liu, T.; Hu, Q.; Zhu, M.; Wang, Z.; Yang, W.; Huang, Z.; Song, W.; Bi, X.; Chen, J.; Sun, Y.; George, C.; Wang, X. Open burning of rice, corn and wheat straws: primary emissions, photochemical aging, and secondary organic aerosol formation. *Atmos. Chem. Phys.* **2017**, *17* (24), 14821−14839.
(11) Hartikainen, A.; Yli-Pirilaä, P.; Tiitta, P.; Leskinen, A.; Kortelainen, M.; Orasche, J. r.; Schnelle-Kreis, J. r.; Lehtinen, K. E.; Zimmermann, R.; Jokiniemi, J.; Sippula, O. Volatile Organic Compounds from Logwood Combustion: Emissions and Transformation under Dark and Photochemical Aging Conditions in a Smog Chamber. *Environ. Sci. Technol.* **2018**, *52* (8), 4979−4988.
(12) Decker, Z. C. J.; Zarzana, K. J.; Coggon, M.; Min, K.-E.; Pollack, I.; Ryerson, T. B.; Peischl, J.; Edwards, P.; Dubé, W. P.; Markovic, M. Z.; Roberts, J. M.; Veres, P. R.; Graus, M.; Warneke, C.; de Gouw, J.; Hatch, L. E.; Barsanti, K. C.; Brown, S. S. Nighttime Chemical Transformation in Biomass Burning Plumes: A Box Model Analysis Initialized with Aircraft Observations. *Environ. Sci. Technol.* **2019**, *53* (5), 2529−2538.
(13) Ciccioli, P.; Brancaleoni, E.; Frattoni, M.; Cecinato, A.; Pinciarelli, L. Determination of volatile organic compounds (VOC) emitted from biomass burning of Mediterranean vegetation species by GC-MS. *Anal. Lett.* **2001**, *34* (6), 937−955.
(14) Gilman, J.; Lerner, B.; Kuster, W.; Goldan, P.; Warneke, C.; Veres, P.; Roberts, J.; de Gouw, J.; Burling, I.; Yokelson, R. Biomass burning emissions and potential air quality impacts of volatile organic compounds and other trace gases from fuels common in the US. *Atmos. Chem. Phys.* **2015**, *15* (24), 13915−13938.
(15) Stockwell, C.; Veres, P.; Williams, J.; Yokelson, R. Characterization of biomass burning emissions from cooking fires, peat, crop residue, and other fuels with high-resolution proton-transfer-reaction time-of-flight mass spectrometry. *Atmos. Chem. Phys.* **2015**, *15* (2), 845−865.
(16) Koss, A. R.; Sekimoto, K.; Gilman, J. B.; Selimovic, V.; Coggon, M. M.; Zarzana, K. J.; Yuan, B.; Lerner, B. M.; Brown, S. S.; Jimenez, J. L.; Krechmer, J.; Roberts, J. M.; Warneke, C.; Yokelson, R. J.; de Gouw, J. Non-methane organic gas emissions from biomass burning: identification, quantification, and emission factors from PTR-ToF during the FIREX 2016 laboratory experiment. *Atmos. Chem. Phys.* **2018**, *18* (5), 3299−3319.
(17) Gomez Alvarez, E. G.; Borrás, E.; Viidanoja, J.; Hjorth, J. Unsaturated dicarbonyl products from the OH-initiated photo-oxidation of furan, 2-methylfuran and 3-methylfuran. *Atmos. Environ.* **2009**, *43* (9), 1603−1612.
(18) Strollo, C. M.; Ziemann, P. J. Products and mechanism of secondary organic aerosol formation from the reaction of 3-methylfuran with OH radicals in the presence of NO x. *Atmos. Environ.* **2013**, *77*, 534−543.
(19) Mettler, M. S.; Mushrif, S. H.; Paulsen, A. D.; Javadekar, A. D.; Vlachos, D. G.; Dauenhauer, P. J. Revealing pyrolysis chemistry for biofuels production: Conversion of cellulose to furans and small oxygenates. *Energy Environ. Sci.* **2012**, *5* (1), 5414−5424.
(20) Mohr, C.; Lopez-Hilfiker, F. D.; Zotter, P.; Prévôt, A. S.; Xu, L.; Ng, N. L.; Herndon, S. C.; Williams, L. R.; Franklin, J. P.; Zahniser, M. S. Contribution of nitrated phenols to wood burning brown carbon light absorption in Detling, United Kingdom during winter time. *Environ. Sci. Technol.* **2013**, *47* (12), 6316−6324.
(21) Iinuma, Y.; Böge, O.; Gräfe, R.; Herrmann, H. Methyl-nitrocatechols: atmospheric tracer compounds for biomass burning secondary organic aerosols. *Environ. Sci. Technol.* **2010**, *44* (22), 8453−8459.
(22) Iinuma, Y.; Keywood, M.; Herrmann, H. Characterization of primary and secondary organic aerosols in Melbourne airshed: The influence of biogenic emissions, wood smoke and bushfires. *Atmos. Environ.* **2016**, *130*, 54−63.
(23) Allan, J.; Williams, P.; Morgan, W.; Martin, C.; Flynn, M.; Lee, J.; Nemitz, E.; Phillips, G.; Gallagher, M.; Coe, H. Contributions from transport, solid fuel burning and cooking to primary organic aerosols in two UK cities. *Atmos. Chem. Phys.* **2010**, *10* (2), 647−668.
(24) Tapia, A.; Villanueva, F.; Salgado, M.; Cabañas, B.; Martínez, E.; Martín, P. Atmospheric degradation of 3-methylfuran: kinetic and products study. *Atmos. Chem. Phys.* **2011**, *11* (7), 3227−3241.
(25) Boyd, C.; Sanchez, J.; Xu, L.; Eugene, A. J.; Nah, T.; Tuet, W.; Guzman, M. I.; Ng, N. Secondary organic aerosol formation from the β-pinene+ NO 3 system: effect of humidity and peroxy radical fate. *Atmos. Chem. Phys.* **2015**, *15* (13), 7497−7522.
(26) Nah, T.; Sanchez, J.; Boyd, C. M.; Ng, N. L. Photochemical Aging of α-pinene and β-pinene Secondary Organic Aerosol formed from Nitrate Radical Oxidation. *Environ. Sci. Technol.* **2016**, *50* (1), 222−231.
(27) Huey, L. G. Measurement of trace atmospheric species by chemical ionization mass spectrometry: Speciation of reactive nitrogen and future directions. *Mass Spectrom. Rev.* **2007**, *26* (2), 166−184.
(28) Zhao, R.; Lee, A.; Abbatt, J. Investigation of aqueous-phase photooxidation of glyoxal and methylglyoxal by aerosol chemical ionization mass spectrometry: observation of hydroxyhydroperoxide formation. *J. Phys. Chem. A* **2012**, *116* (24), 6253−6263.
(29) Aljawhary, D.; Lee, A.; Abbatt, J. High-resolution chemical ionization mass spectrometry (ToF-CIMS): application to study SOA composition and processing. *Atmos. Meas. Tech.* **2013**, *6* (11), 3211.
(30) Lee, B. H.; Lopez-Hilfiker, F. D.; Mohr, C.; Kurtén, T.; Worsnop, D. R.; Thornton, J. A. An iodide-adduct high-resolution time-of-flight chemical-ionization mass spectrometer: Application to atmospheric inorganic and organic compounds. *Environ. Sci. Technol.* **2014**, *48* (11), 6309−6317.
(31) DeCarlo, P. F.; Kimmel, J. R.; Trimborn, A.; Northway, M. J.; Jayne, J. T.; Aiken, A. C.; Gonin, M.; Fuhrer, K.; Horvath, T.; Docherty, K. S.; Worsnop, D. R.; Jimenez, J. L. Field-deployable, high-resolution, time-of-flight aerosol mass spectrometer. *Anal. Chem.* **2006**, *78* (24), 8281−8289.
(32) Canagaratna, M.; Jimenez, J.; Kroll, J.; Chen, Q.; Kessler, S.; Massoli, P.; Hildebrandt Ruiz, L.; Fortner, E.; Williams, L.; Wilson, K.; Surratt, J. D.; Donahue, N. M.; Jayne, J.; Worsnop, D. R. Elemental ratio measurements of organic compounds using aerosol mass spectrometry: characterization, improved calibration, and implications. *Atmos. Chem. Phys.* **2015**, *15* (1), 253−272.
(33) Lopez-Hilfiker, F.; Mohr, C.; Ehn, M.; Rubach, F.; Kleist, E.; Wildt, J.; Mentel, T. F.; Lutz, A.; Hallquist, M.; Worsnop, D.; Thornton, J. A. A novel method for online analysis of gas and particle composition: description and evaluation of a Filter Inlet for Gases and AEROsols (FIGAERO). *Atmos. Meas. Tech.* **2014**, *7* (4), 983−1001.
(34) Stark, H.; Yatavelli, R. L.; Thompson, S. L.; Kang, H.; Krechmer, J. E.; Kimmel, J. R.; Palm, B. B.; Hu, W.; Hayes, P. L.; Day, D. A.; Campuzano-Jost, P.; Canagaratna, M. R.; Jayne, J. T.; Worsnop, D. R.; Jimenez, J. L. Impact of thermal decomposition on thermal desorption instruments: advantage of thermogram analysis for quantifying volatility distributions of organic species. *Environ. Sci. Technol.* **2017**, *51* (15), 8491−8500.
(35) Nah, T.; McVay, R. C.; Pierce, J. R.; Seinfeld, J. H.; Ng, N. L. Constraining uncertainties in particle-wall deposition correction during SOA formation in chamber experiments. *Atmos. Chem. Phys.* **2017**, *17* (3), 2297−2310.
(36) Bahreini, R.; Keywood, M. D.; Ng, N. L.; Varutbangkul, V.; Gao, S.; Flagan, R. C.; Seinfeld, J. H.; Worsnop, D.; Jimenez, J. Measurements of secondary organic aerosol from oxidation of cycloalkenes, terpenes, and m-xylene using an Aerodyne aerosol mass spectrometer. *Environ. Sci. Technol.* **2005**, *39* (15), 5674−5688.

DOI: 10.1021/acsearthspacechem.9b00068
ACS Earth Space Chem. XXXX, XXX, XXX−XXX

(37) McMurry, P. H.; Grosjean, D. Gas and aerosol wall losses in Teflon film smog chambers. *Environ. Sci. Technol.* **1985**, *19* (12), 1176−1182.
(38) Krechmer, J. E.; Pagonis, D.; Ziemann, P. J.; Jimenez, J. L. Quantification of gas-wall partitioning in Teflon environmental chambers using rapid bursts of low-volatility oxidized species generated in situ. *Environ. Sci. Technol.* **2016**, *50* (11), 5757−5765.
(39) Matsunaga, A.; Ziemann, P. J. Gas-wall partitioning of organic compounds in a Teflon film chamber and potential effects on reaction product and aerosol yield measurements. *Aerosol Sci. Technol.* **2010**, *44* (10), 881−892.
(40) Zhang, X.; Cappa, C. D.; Jathar, S. H.; McVay, R. C.; Ensberg, J. J.; Kleeman, M. J.; Seinfeld, J. H. Influence of vapor wall loss in laboratory chambers on yields of secondary organic aerosol. *Proc. Natl. Acad. Sci. U. S. A.* **2014**, *111* (16), 5802−5807.
(41) Nah, T.; McVay, R. C.; Zhang, X.; Boyd, C. M.; Seinfeld, J. H.; Ng, N. L. Influence of seed aerosol surface area and oxidation rate on vapor wall deposition and SOA mass yields: a case study with α-pinene ozonolysis. *Atmos. Chem. Phys.* **2016**, *16* (14), 9361−9379.
(42) Odum, J. R.; Hoffmann, T.; Bowman, F.; Collins, D.; Flagan, R. C.; Seinfeld, J. H. Gas/particle partitioning and secondary organic aerosol yields. *Environ. Sci. Technol.* **1996**, *30* (8), 2580−2585.
(43) Odum, J. R.; Jungkamp, T.; Griffin, R.; Flagan, R. C.; Seinfeld, J. H. The atmospheric aerosol-forming potential of whole gasoline vapor. *Science* **1997**, *276* (5309), 96−99.
(44) Donahue, N.; Robinson, A.; Stanier, C.; Pandis, S. Coupled partitioning, dilution, and chemical aging of semivolatile organics. *Environ. Sci. Technol.* **2006**, *40* (8), 2635−2643.
(45) Ng, N.; Kwan, A.; Surratt, J.; Chan, A.; Chhabra, P.; Sorooshian, A.; Pye, H. O.; Crounse, J.; Wennberg, P.; Flagan, R.; Seinfeld, J. H. Secondary organic aerosol (SOA) formation from reaction of isoprene with nitrate radicals (NO 3). *Atmos. Chem. Phys.* **2008**, *8* (14), 4117−4140.
(46) Ng, N. L.; Kroll, J. H.; Keywood, M. D.; Bahreini, R.; Varutbangkul, V.; Flagan, R. C.; Seinfeld, J. H.; Lee, A.; Goldstein, A. H. Contribution of first-versus second-generation products to secondary organic aerosols formed in the oxidation of biogenic hydrocarbons. *Environ. Sci. Technol.* **2006**, *40* (7), 2283−2297.
(47) Robinson, N. H.; Hamilton, J. F.; Allan, J. D.; Langford, B.; Oram, D. E.; Chen, Q.; Docherty, K.; Farmer, D. K.; Jimenez, J. L.; Ward, M. W.; Hewitt, C. N.; Barley, M. H.; Jenkin, M. E.; Rickard, A. R.; Martin, S. T.; McFiggans, G.; Coe, H. Evidence for a significant proportion of Secondary Organic Aerosol from isoprene above a maritime tropical forest. *Atmos. Chem. Phys.* **2011**, *11* (3), 1039−1050.
(48) Nguyen, T. B.; Coggon, M. M.; Bates, K. H.; Zhang, X.; Schwantes, R. H.; Schilling, K. A.; Loza, C. L.; Flagan, R. C.; Wennberg, P. O.; Seinfeld, J. H. Organic aerosol formation from the reactive uptake of isoprene epoxydiols (IEPOX) onto non-acidified inorganic seeds. *Atmos. Chem. Phys.* **2014**, *14* (7), 3497−3510.
(49) Lin, Y.-H.; Zhang, Z.; Docherty, K. S.; Zhang, H.; Budisulistiorini, S. H.; Rubitschun, C. L.; Shaw, S. L.; Knipping, E. M.; Edgerton, E. S.; Kleindienst, T. E.; Gold, A.; Surratt, J. D. Isoprene epoxydiols as precursors to secondary organic aerosol formation: acid-catalyzed reactive uptake studies with authentic compounds. *Environ. Sci. Technol.* **2012**, *46* (1), 250−258.
(50) Budisulistiorini, S. H.; Canagaratna, M. R.; Croteau, P. L.; Marth, W. J.; Baumann, K.; Edgerton, E. S.; Shaw, S. L.; Knipping, E. M.; Worsnop, D. R.; Jayne, J. T.; Gold, A.; Surratt, J. D. Real-time continuous characterization of secondary organic aerosol derived from isoprene epoxydiols in downtown Atlanta, Georgia, using the Aerodyne Aerosol Chemical Speciation Monitor. *Environ. Sci. Technol.* **2013**, *47* (11), 5686−5694.
(51) Xu, L.; Suresh, S.; Guo, H.; Weber, R. J.; Ng, N. L. Aerosol characterization over the southeastern United States using high-resolution aerosol mass spectrometry: spatial and seasonal variation of aerosol composition and sources with a focus on organic nitrates. *Atmos. Chem. Phys.* **2015**, *15* (13), 7307−7336.
(52) Hu, W. W.; Campuzano-Jost, P.; Palm, B. B.; Day, D. A.; Ortega, A. M.; Hayes, P. L.; Krechmer, J. E.; Chen, Q.; Kuwata, M.; Liu, Y. J.; de Sá, S. S.; McKinney, K.; Martin, S. T.; Hu, M.; Budisulistiorini, S. H.; Riva, M.; Surratt, J. D.; St. Clair, J. M.; Isaacman-Van Wertz, G.; Yee, L. D.; Goldstein, A. H.; Carbone, S.; Brito, J.; Artaxo, P.; de Gouw, J. A.; Koss, A.; Wisthaler, A.; Mikoviny, T.; Karl, T.; Kaser, L.; Jud, W.; Hansel, A.; Docherty, K. S.; Alexander, M. L.; Robinson, N. H.; Coe, H.; Allan, J. D.; Canagaratna, M. R.; Paulot, F.; Jimenez, J. L. Characterization of a real-time tracer for isoprene epoxydiols-derived secondary organic aerosol (IEPOX-SOA) from aerosol mass spectrometer measurements. *Atmos. Chem. Phys.* **2015**, *15* (20), 11807−11833.
(53) Liu, Y.; Kuwata, M.; Strick, B. F.; Geiger, F. M.; Thomson, R. J.; McKinney, K. A.; Martin, S. T. Uptake of epoxydiol isomers accounts for half of the particle-phase material produced from isoprene photooxidation via the HO2 pathway. *Environ. Sci. Technol.* **2015**, *49* (1), 250−258.
(54) Alfarra, M. R.; Coe, H.; Allan, J. D.; Bower, K. N.; Boudries, H.; Canagaratna, M. R.; Jimenez, J. L.; Jayne, J. T.; Garforth, A. A.; Li, S.-M.; Worsnop, D. R. Characterization of urban and rural organic particulate in the lower Fraser valley using two aerodyne aerosol mass spectrometers. *Atmos. Environ.* **2004**, *38* (34), 5745−5758.
(55) Duplissy, J.; DeCarlo, P. F.; Dommen, J.; Alfarra, M. R.; Metzger, A.; Barmpadimos, I.; Prevot, A. S. H.; Weingartner, E.; Tritscher, T.; Gysel, M.; Aiken, A. C.; Jimenez, J. L.; Canagaratna, M. R.; Worsnop, D. R.; Collins, D. R.; Tomlinson, J.; Baltensperger, U. Relating hygroscopicity and composition of organic aerosol particulate matter. *Atmos. Chem. Phys.* **2011**, *11* (3), 1155−1165.
(56) Marcolli, C.; Canagaratna, M. R.; Worsnop, D. R.; Bahreini, R.; de Gouw, J. A.; Warneke, C.; Goldan, P. D.; Kuster, W. C.; Williams, E. J.; Lerner, B. M.; Roberts, J. M.; Meagher, J. F.; Fehsenfeld, F. C.; Marchewka, M.; Bertman, S. B.; Middlebrook, A. M. Cluster Analysis of the Organic Peaks in Bulk Mass Spectra Obtained During the 2002 New England Air Quality Study with an Aerodyne Aerosol Mass Spectrometer. *Atmos. Chem. Phys.* **2006**, *6* (12), 5649−5666.
(57) Ng, N.; Canagaratna, M.; Jimenez, J.; Chhabra, P.; Seinfeld, J.; Worsnop, D. Changes in organic aerosol composition with aging inferred from aerosol mass spectra. *Atmos. Chem. Phys.* **2011**, *11* (13), 6465−6474.
(58) Fry, J.; Kiendler-Scharr, A.; Rollins, A.; Wooldridge, P.; Brown, S.; Fuchs, H.; Dubé, W.; Mensah, A.; Maso, M. d.; Tillmann, R. Organic nitrate and secondary organic aerosol yield from NO 3 oxidation of β-pinene evaluated using a gas-phase kinetics/aerosol partitioning model. *Atmos. Chem. Phys.* **2009**, *9* (4), 1431−1449.
(59) Farmer, D.; Matsunaga, A.; Docherty, K.; Surratt, J.; Seinfeld, J.; Ziemann, P.; Jimenez, J. Response of an aerosol mass spectrometer to organonitrates and organosulfates and implications for atmospheric chemistry. *Proc. Natl. Acad. Sci. U. S. A.* **2010**, *107* (15), 6670−6675.
(60) Bruns, E. A.; Perraud, V. r.; Zelenyuk, A.; Ezell, M. J.; Johnson, S. N.; Yu, Y.; Imre, D.; Finlayson-Pitts, B. J.; Alexander, M. L. Comparison of FTIR and particle mass spectrometry for the measurement of particulate organic nitrates. *Environ. Sci. Technol.* **2010**, *44* (3), 1056−1061.
(61) Ng, N. L.; Brown, S. S.; Archibald, A. T.; Atlas, E.; Cohen, R. C.; Crowley, J. N.; Day, D. A.; Donahue, N. M.; Fry, J. L.; Fuchs, H.; Griffin, R. J.; Guzman, M. I.; Herrmann, H.; Hodzic, A.; Iinuma, Y.; Jimenez, J. L.; Kiendler-Scharr, A.; Lee, B. H.; Luecken, D. J.; Mao, J.; McLaren, R.; Mutzel, A.; Osthoff, H. D.; Ouyang, B.; Picquet-Varrault, B.; Platt, U.; Pye, H. O. T.; Rudich, Y.; Schwantes, R. H.; Shiraiwa, M.; Stutz, J.; Thornton, J. A.; Tilgner, A.; Williams, B. J.; Zaveri, R. A. Nitrate radicals and biogenic volatile organic compounds: oxidation, mechanisms, and organic aerosol. *Atmos. Chem. Phys.* **2017**, *17* (3), 2103−2162.
(62) Boyd, C. M.; Nah, T.; Xu, L.; Berkemeier, T.; Ng, N. L. Secondary Organic Aerosol (SOA) from Nitrate Radical Oxidation of Monoterpenes: Effects of Temperature, Dilution, and Humidity on Aerosol Formation, Mixing, and Evaporation. *Environ. Sci. Technol.* **2017**, *51* (14), 7831−7841.

DOI: 10.1021/acsearthspacechem.9b00068
ACS Earth Space Chem. XXXX, XXX, XXX−XXX

(63) Lopez-Hilfiker, F.; Mohr, C.; D'Ambro, E. L.; Lutz, A.; Riedel, T. P.; Gaston, C. J.; Iyer, S.; Zhang, Z.; Gold, A.; Surratt, J. D.; Lee, B. H.; Kurten, T.; Hu, W. W.; Jimenez, J. L.; Hallquist, M.; Thornton, J. A. Molecular composition and volatility of organic aerosol in the Southeastern US: implications for IEPOX derived SOA. *Environ. Sci. Technol.* **2016**, *50* (5), 2200−2209.
(64) Lopez-Hilfiker, F.; Mohr, C.; Ehn, M.; Rubach, F.; Kleist, E.; Wildt, J.; Mentel, T. F.; Carrasquillo, A.; Daumit, K.; Hunter, J.; Kroll, J. H.; Worsnop, D. R.; Thornton, J. A. Phase partitioning and volatility of secondary organic aerosol components formed from α-pinene ozonolysis and OH oxidation: the importance of accretion products and other low volatility compounds. *Atmos. Chem. Phys.* **2015**, *15* (14), 7765−7776.
(65) Ehn, M.; Thornton, J. A.; Kleist, E.; Sipilä, M.; Junninen, H.; Pullinen, I.; Springer, M.; Rubach, F.; Tillmann, R.; Lee, B. A large source of low-volatility secondary organic aerosol. *Nature* **2014**, *506* (7489), 476.
(66) Faxon, C.; Hammes, J.; Breton, M. L.; Pathak, R. K.; Hallquist, M. Characterization of organic nitrate constituents of secondary organic aerosol (SOA) from nitrate-radical-initiated oxidation of limonene using high-resolution chemical ionization mass spectrometry. *Atmos. Chem. Phys.* **2018**, *18* (8), 5467−5481.
(67) Zhang, W.; Du, B.; Mu, L.; Feng, C. Mechanism for the gas-phase reaction between OH and 3-methylfuran: A theoretical study. *Int. J. Quantum Chem.* **2008**, *108* (7), 1232−1238.
(68) Bierbach, A.; Barnes, I.; Becker, K. Product and kinetic study of the OH-initiated gas-phase oxidation of furan, 2-methylfuran and furanaldehydes at$\asymp$ 300 K. *Atmos. Environ.* **1995**, *29* (19), 2651−2660.
(69) Aschmann, S. M.; Nishino, N.; Arey, J.; Atkinson, R. Products of the OH Radical-Initiated Reactions of Furan, 2-and 3-Methylfuran, and 2, 3-and 2, 5-Dimethylfuran in the Presence of NO. *J. Phys. Chem. A* **2014**, *118* (2), 457−466.
(70) Rayez, M.-T. r. s.; Rayez, J.-C.; Kerdouci, J.; Picquet-Varrault, B. n. d. Theoretical study of the gas-phase reactions of NO3 radical with a series of trans-2-unsaturated aldehydes: from acrolein to trans-2-octenal. *J. Phys. Chem. A* **2014**, *118* (28), 5149−5155.
(71) Russell, G. A. Deuterium-isotope effects in the autoxidation of aralkyl hydrocarbons. mechanism of the interaction of peroxy radicals1. *J. Am. Chem. Soc.* **1957**, *79* (14), 3871−3877.
(72) Claflin, M. S.; Ziemann, P. J. Identification and Quantitation of Aerosol Products of the Reaction of β-Pinene with NO3 Radicals and Implications for Gas-and Particle-Phase Reaction Mechanisms. *J. Phys. Chem. A* **2018**, *122* (14), 3640−3652.
(73) Wang, D. S.; Ruiz, L. H. Chlorine-initiated oxidation of n-alkanes under high NOx conditions: Insights into secondary organic aerosol composition and volatility using a FIGAERO-CIMS. *Atmos. Chem. Phys. Discuss.* **2018**, 1.
(74) Pankow, J. F.; Asher, W. E. SIMPOL. 1: a simple group contribution method for predicting vapor pressures and enthalpies of vaporization of multifunctional organic compounds. *Atmos. Chem. Phys.* **2008**, *8* (10), 2773−2796.
(75) Kroll, J. H.; Seinfeld, J. H. Chemistry of secondary organic aerosol: Formation and evolution of low-volatility organics in the atmosphere. *Atmos. Environ.* **2008**, *42* (16), 3593−3624.
(76) Ziemann, P. J.; Atkinson, R. Kinetics, products, and mechanisms of secondary organic aerosol formation. *Chem. Soc. Rev.* **2012**, *41* (19), 6582−6605.
(77) Dibble, T. S. Failures and limitations of quantum chemistry for two key problems in the atmospheric chemistry of peroxy radicals. *Atmos. Environ.* **2008**, *42* (23), 5837−5848.
(78) Kan, C. S.; Calvert, J. G.; Shaw, J. H. Reactive channels of the methyldioxy-methyldioxy reaction. *J. Phys. Chem.* **1980**, *84* (25), 3411−3417.
(79) Niki, H.; Maker, P.; Savage, C.; Breitenbach, L. Fourier-transform infrared studies of the self-reaction of CH3O2 radicals. *J. Phys. Chem.* **1981**, *85* (7), 877−881.
(80) Tyndall, G.; Cox, R.; Granier, C.; Lesclaux, R.; Moortgat, G.; Pilling, M.; Ravishankara, A.; Wallington, T. Atmospheric chemistry of small organic peroxy radicals. *Journal of Geophysical Research: Atmospheres.* **2001**, *106* (D11), 12157−12182.
(81) Kwan, A.; Chan, A.; Ng, N.; Kjærgaard, H. G.; Seinfeld, J.; Wennberg, P. Peroxy radical chemistry and OH radical production during the NO 3-initiated oxidation of isoprene. *Atmos. Chem. Phys.* **2012**, *12* (16), 7499−7515.
(82) Claflin, M. S.; Krechmer, J. E.; Hu, W.; Jimenez, J. L.; Ziemann, P. J. Functional Group Composition of Secondary Organic Aerosol Formed from Ozonolysis of α-Pinene Under High VOC and Autoxidation Conditions. *ACS Earth and Space Chemistry.* **2018**, *2* (11), 1196−1210.
(83) Jimenez, J. L.; Canagaratna, M. R.; Donahue, N. M.; Prevot, A. S. H.; Zhang, Q.; Kroll, J. H.; DeCarlo, P. F.; Allan, J. D.; Coe, H.; Ng, N. L.; Aiken, A. C.; Docherty, K. S.; Ulbrich, I. M.; Grieshop, A. P.; Robinson, A. L.; Duplissy, J.; Smith, J. D.; Wilson, K. R.; Lanz, V. A.; Hueglin, C.; Sun, Y. L.; Tian, J.; Laaksonen, A.; Raatikainen, T.; Rautiainen, J.; Vaattovaara, P.; Ehn, M.; Kulmala, M.; Tomlinson, J. M.; Collins, D. R.; Cubison, M. J.; Dunlea, J.; Huffman, J. A.; Onasch, T. B.; Alfarra, M. R.; Williams, P. I.; Bower, K.; Kondo, Y.; Schneider, J.; Drewnick, F.; Borrmann, S.; Weimer, S.; Demerjian, K.; Salcedo, D.; Cottrell, L.; Griffin, R.; Takami, A.; Miyoshi, T.; Hatakeyama, S.; Shimono, A.; Sun, J. Y.; Zhang, Y. M.; Dzepina, K.; Kimmel, J. R.; Sueper, D.; Jayne, J. T.; Herndon, S. C.; Trimborn, A. M.; Williams, L. R.; Wood, E. C.; Middlebrook, A. M.; Kolb, C. E.; Baltensperger, U.; Worsnop, D. R. Evolution of Organic Aerosols in the Atmosphere. *Science* **2009**, *326* (5959), 1525−1529.
(84) Huffman, J.; Docherty, K.; Aiken, A.; Cubison, M.; Ulbrich, I.; DeCarlo, P.; Sueper, D.; Jayne, J.; Worsnop, D.; Ziemann, P. Chemically-resolved aerosol volatility measurements from two megacity field studies. *Atmos. Chem. Phys.* **2009**, *9* (18), 7161−7182.
(85) Ulbrich, I.; Canagaratna, M.; Zhang, Q.; Worsnop, D.; Jimenez, J. Interpretation of organic components from Positive Matrix Factorization of aerosol mass spectrometric data. *Atmos. Chem. Phys.* **2009**, *9* (9), 2891−2918.
(86) Aiken, A. C.; DeCarlo, P. F.; Kroll, J. H.; Worsnop, D. R.; Huffman, J. A.; Docherty, K. S.; Ulbrich, I. M.; Mohr, C.; Kimmel, J. R.; Sueper, D.; Sun, Y.; Zhang, Q.; Trimborn, A.; Northway, M.; Ziemann, P. J.; Canagaratna, M. R.; Onasch, T. B.; Alfarra, M. R.; Prevot, A. S. H.; Dommen, J.; Duplissy, J.; Metzger, A.; Baltensperger, U.; Jimenez, J. L. O/C and OM/OC Ratios of Primary, Secondary, and Ambient Organic Aerosols with High-Resolution Time-of-Flight Aerosol Mass Spectrometry. *Environ. Sci. Technol.* **2008**, *42* (12), 4478−4485.
(87) Fry, J. L.; Draper, D. C.; Zarzana, K. J.; Campuzano-Jost, P.; Day, D. A.; Jimenez, J. L.; Brown, S. S.; Cohen, R. C.; Kaser, L.; Hansel, A.; Cappellin, L.; Karl, T.; Hodzic Roux, A.; Turnipseed, A.; Cantrell, C.; Lefer, B. L.; Grossberg, N. Observations of gas- and aerosol-phase organic nitrates at BEACHON-RoMBAS 2011. *Atmos. Chem. Phys.* **2013**, *13* (17), 8585−8605.
(88) Fry, J. L.; Draper, D. C.; Barsanti, K. C.; Smith, J. N.; Ortega, J.; Winkler, P. M.; Lawler, M. J.; Brown, S. S.; Edwards, P. M.; Cohen, R. C.; Lee, L. Secondary organic aerosol formation and organic nitrate yield from NO3 oxidation of biogenic hydrocarbons. *Environ. Sci. Technol.* **2014**, *48* (20), 11944−11953.
(89) Seinfeld, J. H.; Pandis, S. N. *Atmospheric Chemistry and Physics: from Air Pollution to Climate Change*; John Wiley & Sons: 2016.
(90) Donahue, N. M.; Kroll, J.; Pandis, S. N.; Robinson, A. L. A two-dimensional volatility basis set−Part 2: Diagnostics of organic-aerosol evolution. *Atmos. Chem. Phys.* **2012**, *12* (2), 615−634.
(91) Robinson, A. L.; Donahue, N. M.; Shrivastava, M. K.; Weitkamp, E. A.; Sage, A. M.; Grieshop, A. P.; Lane, T. E.; Pierce, J. R.; Pandis, S. N. Rethinking organic aerosols: Semivolatile emissions and photochemical aging. *Science* **2007**, *315* (5816), 1259−1262.
(92) Hu, W.; Palm, B. B.; Day, D. A.; Campuzano-Jost, P.; Krechmer, J. E.; Peng, Z.; de Sá, S. S.; Martin, S. T.; Alexander, M. L.; Baumann, K.; Hacker, L.; Kiendler-Scharr, A.; Koss, A. R.; de Gouw, J. A.; Goldstein, A. H.; Seco, R.; Sjostedt, S. J.; Park, J. H.; Guenther, A. B.; Kim, S.; Canonaco, F.; Prévôt, A. S. H.; Brune, W. H.; Jimenez,

DOI: 10.1021/acsearthspacechem.9b00068
ACS Earth Space Chem. XXXX, XXX, XXX−XXX

J. L. Volatility and lifetime against OH heterogeneous reaction of ambient isoprene-epoxydiols-derived secondary organic aerosol (IEPOX-SOA). *Atmos. Chem. Phys.* **2016**, *16* (18), 11563−11580.
(93) Cappa, C.; Jimenez, J. Quantitative estimates of the volatility of ambient organic aerosol. *Atmos. Chem. Phys.* **2010**, *10* (12), 5409−5424.
(94) Kostenidou, E.; Karnezi, E.; Hite Jr, J. R.; Bougiatioti, A.; Cerully, K.; Xu, L.; Ng, N. L.; Nenes, A.; Pandis, S. N. Organic aerosol in the summertime southeastern United States: components and their link to volatility distribution, oxidation state and hygroscopicity. *Atmos. Chem. Phys.* **2018**, *18* (8), 5799−5819.
(95) Saha, P. K.; Grieshop, A. P. Exploring divergent volatility properties from yield and thermodenuder measurements of secondary organic aerosol from α-pinene ozonolysis. *Environ. Sci. Technol.* **2016**, *50* (11), 5740−5749.
(96) Häkkinen, S.; Äijälä, M.; Lehtipalo, K.; Junninen, H.; Backman, J.; Virkkula, A.; Nieminen, T.; Vestenius, M.; Hakola, H.; Ehn, M.; Worsnop, D. R.; Kulmala, M.; Petäjä, T.; Riipinen, I. Long-term volatility measurements of submicron atmospheric aerosol in Hyytiälä, Finland. *Atmos. Chem. Phys.* **2012**, *12* (22), 10771−10786.
(97) Hatch, L. E.; Luo, W.; Pankow, J. F.; Yokelson, R. J.; Stockwell, C. E.; Barsanti, K. Identification and quantification of gaseous organic compounds emitted from biomass burning using two-dimensional gas chromatography−time-of-flight mass spectrometry. *Atmos. Chem. Phys.* **2015**, *15* (4), 1865−1899.
(98) Xu, L.; Guo, H.; Weber, R. J.; Ng, N. L. Chemical characterization of water-soluble organic aerosol in contrasting rural and urban environments in the southeastern United States. *Environ. Sci. Technol.* **2017**, *51* (1), 78−88.
(99) Alvarado, M. J.; Logan, J. A.; Mao, J.; Apel, E.; Riemer, D.; Blake, D.; Cohen, R. C.; Min, K. E.; Perring, A. E.; Browne, E. C.; Wooldridge, P. J.; Diskin, G. S.; Sachse, G. W.; Fuelberg, H.; Sessions, W. R.; Harrigan, D. L.; Huey, G.; Liao, J.; Case-Hanks, A.; Jimenez, J. L.; Cubison, M. J.; Vay, S. A.; Weinheimer, A. J.; Knapp, D. J.; Montzka, D. D.; Flocke, F. M.; Pollack, I. B.; Wennberg, P. O.; Kurten, A.; Crounse, J.; Clair, J. M. S.; Wisthaler, A.; Mikoviny, T.; Yantosca, R. M.; Carouge, C. C.; Le Sager, P. Nitrogen oxides and PAN in plumes from boreal fires during ARCTAS-B and their impact on ozone: an integrated analysis of aircraft and satellite observations. *Atmos. Chem. Phys.* **2010**, *10* (20), 9739−9760.
(100) Akagi, S. K.; Craven, J. S.; Taylor, J. W.; McMeeking, G. R.; Yokelson, R. J.; Burling, I. R.; Urbanski, S. P.; Wold, C. E.; Seinfeld, J. H.; Coe, H.; Alvarado, M. J.; Weise, D. R. Evolution of trace gases and particles emitted by a chaparral fire in California. *Atmos. Chem. Phys.* **2012**, *12* (3), 1397−1421.
(101) Cubison, M. J.; Ortega, A. M.; Hayes, P. L.; Farmer, D. K.; Day, D.; Lechner, M. J.; Brune, W. H.; Apel, E.; Diskin, G. S.; Fisher, J. A.; Fuelberg, H. E.; Hecobian, A.; Knapp, D. J.; Mikoviny, T.; Riemer, D.; Sachse, G. W.; Sessions, W.; Weber, R. J.; Weinheimer, A. J.; Wisthaler, A.; Jimenez, J. L. Effects of aging on organic aerosol from open biomass burning smoke in aircraft and laboratory studies. *Atmos. Chem. Phys.* **2011**, *11* (23), 12049−12064.
(102) Jolleys, M. D.; Coe, H.; McFiggans, G.; Capes, G.; Allan, J. D.; Crosier, J.; Williams, P. I.; Allen, G.; Bower, K. N.; Jimenez, J. L.; Russell, L. M.; Grutter, M.; Baumgardner, D. Characterizing the aging of biomass burning organic aerosol by use of mixing ratios: a meta-analysis of four regions. *Environ. Sci. Technol.* **2012**, *46* (24), 13093−13102.
(103) Capes, G.; Johnson, B.; McFiggans, G.; Williams, P.; Haywood, J.; Coe, H. Aging of biomass burning aerosols over West Africa: Aircraft measurements of chemical composition, microphysical properties, and emission ratios. *J. Geophys. Res.* **2008**, *113*, D00C15.
(104) Forrister, H.; Liu, J.; Scheuer, E.; Dibb, J.; Ziemba, L.; Thornhill, K. L.; Anderson, B.; Diskin, G.; Perring, A. E.; Schwarz, J. P.; Campuzano-Jost, P.; Day, D.; Palm, B.; Jimenez, J. L.; Nenes, A.; Weber, R. J. Evolution of brown carbon in wildfire plumes. *Geophys. Res. Lett.* **2015**, *42* (11), 4623−4630.
(105) Shrivastava, M.; Cappa, C. D.; Fan, J.; Goldstein, A. H.; Guenther, A. B.; Jimenez, J. L.; Kuang, C.; Laskin, A.; Martin, S. T.; Ng, N. L.; Petaja, T.; Pierce, J. R.; Rasch, P. J.; Roldin, P.; Seinfeld, J. H.; Shilling, J.; Smith, J. N.; Thornton, J. A.; Volkamer, R.; Wang, J.; Worsnop, D. R.; Zaveri, R. A.; Zelenyuk, A.; Zhang, Q. Recent advances in understanding secondary organic aerosol: Implications for global climate forcing. *Rev. Geophys.* **2017**, *55* (2), 509−559.

DOI: 10.1021/acsearthspacechem.9b00068
ACS Earth Space Chem. XXXX, XXX, XXX−XXX